



Gyrospon antimicrobial nanoparticle loaded fibrous polymeric filters



U. Eranka Illangakoon^a, S. Mahalingam^a, K. Wang^a, Y.-K. Cheong^b, E. Canales^d, G.G. Ren^b, E. Cloutman-Green^c, M. Edirisinghe^{a,*}, L. Ciric^d

^a Department of Mechanical Engineering, University College London, London WC1E 7JE, UK

^b School of Engineering and Technology, University of Hertfordshire, Hatfield AL10 9AB, UK

^c Department of Microbiology, Virology, and Infection Prevention Control, Great Ormond Street Hospital NHS Foundation Trust, London WC1N 3JH, UK

^d Department of Civil, Environmental and Geomatic Engineering, University College London, London WC1E 7JE, UK

ARTICLE INFO

Article history:

Received 18 November 2016

Accepted 4 December 2016

Available online 7 December 2016

Keywords:

Gyrospon

Fibres

Filters

Nanoparticle

Antimicrobial

ABSTRACT

A one step approach to prepare hybrid nanoparticle embedded polymer fibres using pressurised gyration is presented. Two types of novel antimicrobial nanoparticles and poly(methylmethacrylate) polymer were used in this work. X-ray diffraction analysis of the nanoparticles revealed Ag, Cu and W are the main elements present in them. The concentration of the polymer solution and the nanoparticle concentration had a significant influence on the fibre diameter, pore size and morphology. Fibres with a diameter in the range of 6–20 µm were spun using 20 wt% polymer solutions containing 0.1, 0.25 and 0.5 wt% nanoparticles under 0.3 MPa working pressure and a rotational speed of 36,000 rpm. Continuous, bead-free fibre morphologies were obtained for each case. The pore size in the fibres varied between 36 and 300 nm. Successful incorporation of the nanoparticles in polymer fibres was confirmed by energy dispersive x-ray analysis. The fibres were also gyrospon on to metallic discs to prepare filters which were tested for their antibacterial activity on a suspension of *Pseudomonas aeruginosa*. Nanoparticle loaded fibres showed higher antibacterial efficacy than pure poly(methylmethacrylate) fibres.

© 2016 The Authors. Published by Elsevier B.V. This is an open access article under the CC BY license (<http://creativecommons.org/licenses/by/4.0/>).

1. Introduction

Hospital acquired infections (HAIs), often caused by drug-resistant organisms, are causing notable mortality and morbidity in patients and an upshot in a social and economic burden [1]. Thus there is a growing demand to find new ways to minimise the transmission of infection more effectively and efficiently. Currently many hospitals employ 'point of use' filters at water outlets to remove microbes from the water flow [2]. However, these filters only serve to trap bacteria and not kill them. Consequently, biofilms can form in these filters and bacteria continue to live there, potentially acting as a continuous source of pathogens particularly in vulnerable patients who are already immunocompromised [3]. One common microbe found in hospital water systems is *Pseudomonas aeruginosa*, of which a number of outbreaks have been reported [4,5].

Nanoparticles of metals and their compounds have attracted the interest of many communities over the years for many reasons. In particular, Ag and Cu nanoparticles, both show excellent antimicrobial properties [6,7]. In the biomedical field, Ag has been used widely in medical care - for medical devices, water purification and antimicrobial uses. It shows favourable biocompatibility and has been shown to be relatively non-toxic and inert to mammalian cells and tissue [8]. In

addition, Ag has effective antimicrobial effects against both Gram positive bacteria and Gram negative bacteria, including *P. aeruginosa* [9]. Cu has found use in the biomedical industry, with properties attractive for use in medical devices. Not only is it an essential trace element for humans, but in addition the strong antibacterial properties are increasingly being exploited [10]. W is another metal with low toxicity with emerging uses in antimicrobial applications [11]. The functionality of antimicrobial nanoparticles has been increasingly studied for their dispersibility and toxicities with respect to their applications in biomedicine, bio-devices, healthcare and general engineering and to understand mechanisms and biological interactions. The increasing prevalence of HAIs and growing problems of antimicrobial resistant pathogens poses a serious concern in healthcare, and therefore nanoparticles and their potential applications as antimicrobials provide a promising novel approach in prohibiting the spread of such infections [12,13].

In recent years, pressurised gyration and its sister-processes have been extensively utilised as a convenient method to manufacture polymeric nanofibres with a diameter ranging from tens of nanometers to several micrometers [14–22]. This technique has become very popular and has attracted the attention of many researchers worldwide owing to its versatility, robustness and consistency of generating nanofibres on a large scale in a single step [14]. In a typical pressurised gyration operation, a polymer solution (or melt) is rotated at a high angular speed under a pressurised fluid flow in a perforated aluminium cylindrical vessel to eject a multitude of polymer jets through the orifices. Subsequently,

* Corresponding author.

E-mail address: m.edirisinghe@ucl.ac.uk (M. Edirisinghe).

the ejected jets elongate along the circumferential direction due to a combination of centrifugal and dynamic fluid flow forces. Ultimately solvent evaporation takes place resulting in thinner fibres landing on a collector which can be passive or active. The angular speed, fluid pressure, polymer concentration, type of solvent (thus solvent evaporation and solidification) and temperature determines the fibre size, fibre size distribution and surface morphology of the generated fibres [14–22].

The objective of this research was the generation of fibrous filters containing two types of novel antimicrobial nanoparticles (AMNP), 1 and 2, by pressurised gyration and the examination of their antimicrobial potential. These novel nanoparticles have the potential to kill both bacteria and viruses [23]. For this purpose, circular disc shaped filtration membranes were prepared using the nanofibres. The antimicrobial potential of the filtration membranes was studied using the microorganism *P. aeruginosa*, a common HCAI associated with hospital water systems.

2. Materials and methods

2.1. Materials

Poly(methylmethacrylate) (PMMA, M_w 120,000 g/mol) and chloroform were obtained from Sigma-Aldrich (Gillingham, UK). PMMA was selected mainly because of the requirement of a water insoluble polymer for the preparation of the fibrous mats. All reagents were analytical grade and were used as received. Antimicrobial nanoparticles (two types: AMNP1 and AMNP2) were provided by Dr. Guogang Ren of the University of Hertfordshire, UK and the generic details pertaining to their composition and preparation are given elsewhere [23]. AMNP1 and 2 were studied using X-ray diffraction. X-ray diffraction (XRD) patterns were obtained using a MiniFlex 600 diffractometer (Rigaku, Tokyo, Japan) with $\text{CuK}\alpha$ radiation ($\lambda = 1.5148 \text{ \AA}$). Data were recorded over the 2θ range $5\text{--}120^\circ$ at 40 mV and 15 mA.

2.2. Preparation of spinning solutions

20% (w/w) PMMA solution was prepared by dissolving PMMA in chloroform. The polymer solution was magnetically stirred for 24 h to obtain a homogeneous solution and labelled as K0. 0.1%, 0.25% and 0.5% AMNP1 loaded (w/w) PMMA fibres were prepared by adding the required amount of AMNP1 to the PMMA solution and labelled as K1, K2 and K3, respectively. All the three solutions were stirred for 30 min before spinning in order to ensure homogenous distribution of AMNP1. Similarly, AMNP2 loaded PMMA fibres were prepared by adding the required amount of AMNP2 (identical percentages as above) to the PMMA solution and labelled as K4, K5 and K6, containing 0.1%, 0.25% and 0.5% AMNP2 (w/w), respectively.

2.3. Pressurised gyration

Fig. 1a displays a schematic diagram of the pressurised gyration apparatus that was used in this research. The setup consists of a cylindrical aluminium vessel (60 mm in diameter, 30 mm in height) with 24 orifices of 0.5 mm diameter in size. A high speed rotary motor attached to the cylindrical vessel was connected to a circuit board, from which the rotation speed of the vessel could be varied. The pressurised gyration apparatus was placed within a cabinet, which also served as the collection plate placed 100 mm from the vessel for the collection of fibres during initial trails simply to generate AMNP-loaded fibres. The motor could be turned on and off via a remote controller. A 10 ml syringe was used to deposit the polymer solutions into the vessel, and then the lid was attached and tightly screwed in order to prevent polymer solution from escaping via the gap between the lid and the vessel. For all solutions the rotational speed was kept constant at 36,000 rpm (maximum possible) and the applied working pressure was varied

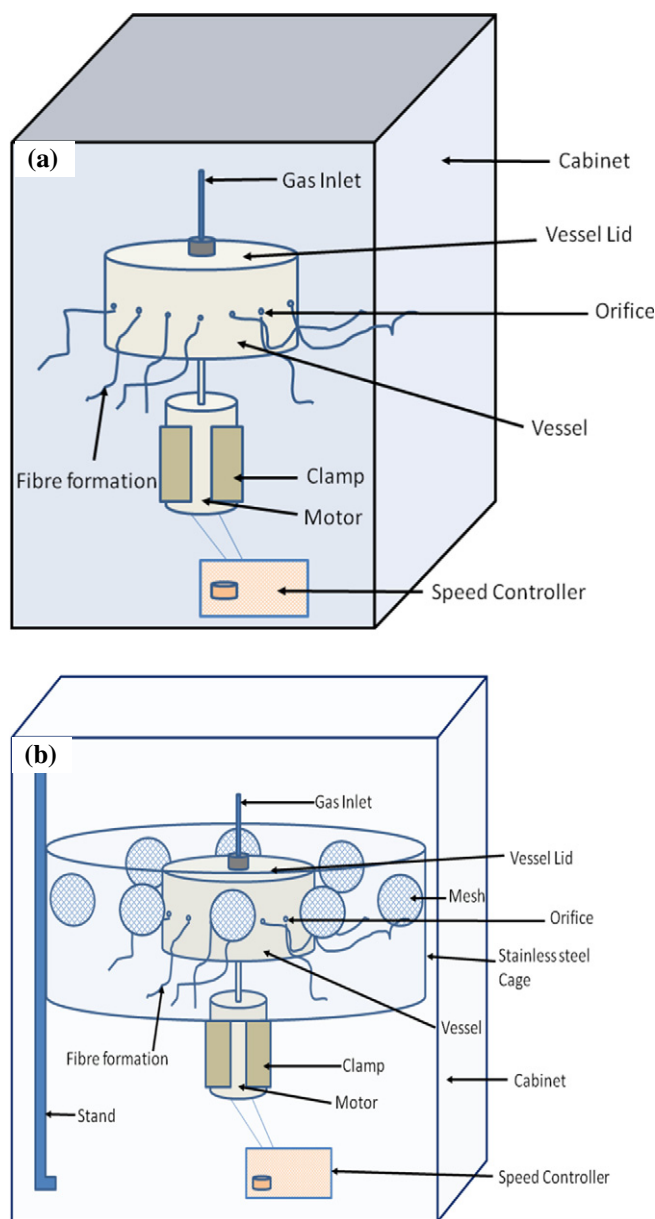


Fig. 1. Schematic diagrams illustrating (a) conventional pressurised gyration rig (b) modified rig to collect fibres on discs.

between 0 and 0.3 MPa to study the influence of working pressure on the fibre forming.

2.4. Fibre deposition on metal discs

Stainless steel discs (31 mm diameter and 0.5 mm thick containing a mesh grid of 2 mm^2 holes) were first sterilized with 95% ethanol and air dried prior to use. The pressurised gyration apparatus was modified to allow for fibre deposition on the discs; a schematic diagram of the modified setup is given in Fig. 1b, where a metal cage (75 mm height by 165 mm diameter) was placed 45 mm away from the vessel, and held in place by a metal stand. The discs were mounted on the metal cage and used to collect the fibres for 300 s, thereby depositing a mat which covered the entirety of the discs. The fibre mats deposited on discs are shown in Fig. 2. No specific experiments carried out to vary and regulate the thickness of the mat in this work, however the thickness was between 1 and 2 μm , making subsequent microbiological experiments comparable. All spinning experiments were done at temperature $22 \pm 2^\circ \text{C}$ and relative humidity was $42 \pm 3\%$.

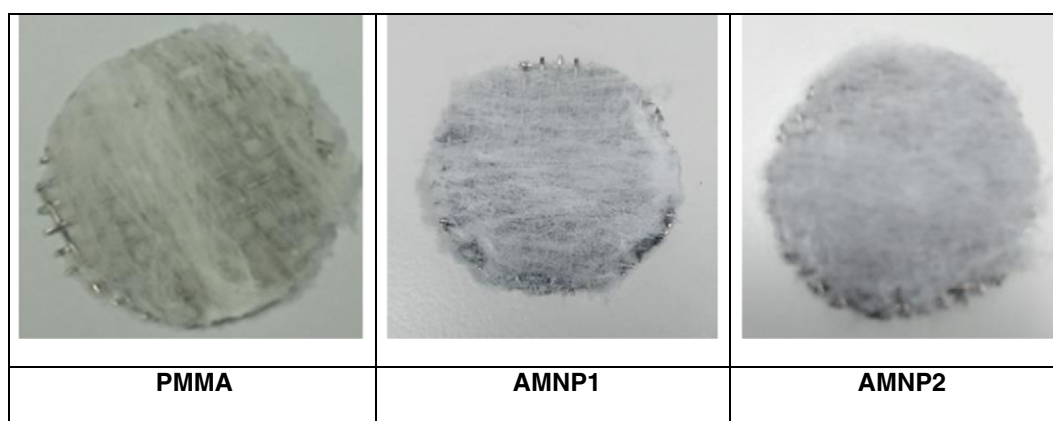


Fig. 2. Fibrous filters deposited on meshed metallic discs to create filters. AMNP1 and 2 concentrations are 0.5% w/w.

2.5. Fibre characterisation

The fibre morphology was assessed using a JEOL JSM-6301F scanning electron microscope (SEM) operated at an accelerating voltage of 5 kV. Prior to imaging, samples were coated using a Quorum Q150R ES sputter coater for 90 s. The average fibre diameter and the average pore size in these fibres were determined by measuring the diameter of more than 50 fibres/pores captured by SEM images using the ImageJ software (National Institutes of Health, Bethesda, MD, USA). The fibre diameter and the pore size of the gyrospon fibres are given in Tables 1 & 2. Energy dispersive X-ray spectroscopy (EDX) was carried out using a Philips XL-30 scanning electron microscope that has an EDX facility in order to identify the presence of the AMNP particles. Samples were carbon coated using Edwards Auto 306 vacuum coater prior to EDX. Three different locations of the sample were randomly selected and scanned for EDX spectra.

2.6. Antibacterial testing

The antibacterial activity of the 0.5% (w/w) AMNP loaded fibre mats containing K3 and K6 fibres (Tables 1 and 2) was assessed using Gram-negative *P. aeruginosa* (strain 25-09071215-05). This was the highest AMNP loading used in this work and we chose to test these only to compare AMNP1 and AMNP2. The cells were cultured in nutrient broth (Oxoid, UK) for 16 h at 30 °C and agitation at 150 rpm. The culture was then centrifuged at 4000 rpm for 15 min, the supernatant discarded and the cells resuspended in 100 ml phosphate buffered saline (PBS, Sigma). The cell suspension in PBS was then passed through the fibre mats deposited on discs as shown in Fig. 2 at a flow rate of 1.67 ml min⁻¹. A sample of the bacterial suspension was taken before and after filtration through the mat. Ten-fold serial dilutions were performed on all samples and these were then plated onto nutrient agar (Oxoid, UK) and incubated at 30 °C for 24 h, after which the number of viable colony-forming units of bacteria was obtained and a reduction due to filtration in viable number was calculated.

3. Results and discussion

3.1. Fibre optimisation

For any fibre spinning process, the processing parameters have to be optimised to generate defect free continuous uniform fibres. One of those parameters is the polymer concentration. For a given polymer, there needs to be a minimum critical concentration, deemed the critical entanglement concentration; if not satisfied fibres cannot be formed [14,21]. Thus finding a suitable viscosity and identifying the critical polymer concentration is a key factor in order to produce uniform fibres successfully. Therefore, PMMA polymer concentration was varied between 5 and 30 wt% in the selected solvent (chloroform) to generate the fibres for the filtration applications.

In addition to polymer concentration, other crucial factors that govern the pressurised gyration process are rotating speed and applied working pressure. It has been shown that increase of rotating speed and working pressure results in thinner fibres [14]. PMMA solutions of 5, 10, 15, 20, 25 and 30 wt% were spun at different processing parameters. 5 wt% and 10 wt% solutions produced few fibres. Both 15 wt% and 20 wt% solutions were able to produce fibres with no applied pressure and applied pressure, with best overall yield. 25 wt% and 30 wt% were not able to form any fibres and instead solidified polymeric bubble relics were formed at the orifices of the vessel. A possible explanation for these observations could be that the higher polymer concentration causes the solvent to evaporate too quickly due to higher polymer to solvent ratio resulting in no fibre formation. It has been suggested that the solution viscosity, which increases with higher polymer loading, is a crucial factor affecting fibre morphology [24]. At low viscosity, smooth and continuous fibres cannot be generated, and at high viscosity the hard ejection of jets occur [24]. Similar observations were found in recent pressure assisted gyration work where a higher polymer concentration/viscosity resulted in stronger shear thinning allowing the generation of various fibre morphologies of polycaprolactone polymer [25]. Ultimately, the 20 wt% was chosen to be the optimum polymer solution to incorporate the AMNP nanoparticles in this work.

Table 1
Fibre diameter and pore data of the AMNP1 containing composite fibres.

Fibre sample	AMNP1 loading (w/w)	Average fibre diameter (µm)	Average pore diameter (nm)
K0	0	20 ± 12	90 ± 8
K1	0.1	19 ± 7	67 ± 26
K2	0.25	8 ± 5	100 ± 27
K3	0.50	6 ± 4	36 ± 18

Table 2
Fibre diameter and pore data of the AMNP2 containing composite fibres.

Fibre sample	AMNP2 loading (w/w)	Average fibre diameter (µm)	Average pore diameter (nm)
K4	0.1	16 ± 7	130 ± 20
K5	0.25	12 ± 5	260 ± 35
K6	0.50	7 ± 4	300 ± 38

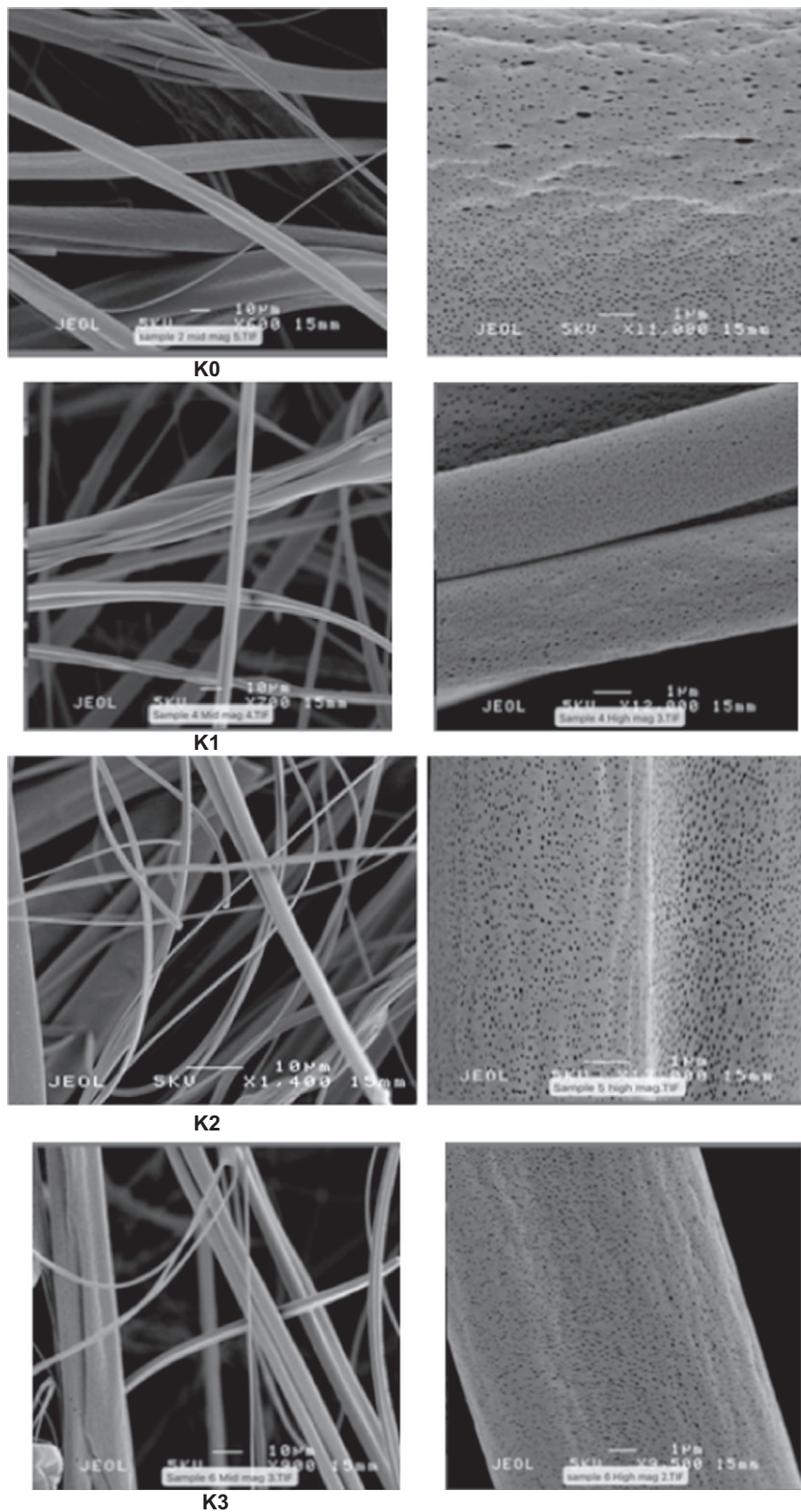


Fig. 3. SEM images of the PMMA and AMNP1 incorporated PMMA fibres obtained at 36,000 rpm rotating speed and 0.3 MPa working pressure. K0, K1, K2 and K3 are defined in Table 1.

3.2. AMNP nanoparticle incorporated PMMA fibres

These fibres were spun at 36,000 rpm rotating speed and 0.3 MPa working pressure using 20 wt% polymer solution and various concentrations of AMNP nanoparticles. The concentration of the particles used was 0.1, 0.25 and 0.5 wt%. Fig. 3 shows SEM images of the AMNP1 loaded fibres spun for each of the samples at higher and lower magnification. It is clearly evident that continuous, smooth bead-free fibres have been produced in all instances. The high magnification images show that surface pores appear in fibres of all the samples, and the pores are evenly distributed on the surface. Table 1 displays characteristics features of the fibres obtained. The fibre diameter is in the range 2–65 μm . Virgin PMMA fibres had an average fibre diameter (AFD) of 20 μm with a standard deviation (SD) of 12 μm . The average pore diameter (APD) of PMMA fibres was 93 nm with a standard deviation (SD) of 50 nm. The pores were in the range 43 nm–548 nm. In contrast, AMNP loaded PMMA showed a varying trend in fibre diameter as the nanoparticle concentration was changed. 0.1% AMNP1 loaded fibres gave AFD of $19 \pm 7 \mu\text{m}$, with a range of 7 μm –55 μm . 0.25% AMNP1 loaded fibres had AFD of $8 \pm 5 \mu\text{m}$, with a range of 1 μm –35 μm . The AFD obtained for 0.5% AMNP1 loaded fibres was $6 \pm 4 \mu\text{m}$, with a range of 1 μm –30 μm .

Fig. 4 shows the high and low magnification images of the AMNP2 loaded PMMA fibres spun at 36,000 rpm rotating speed and 0.3 MPa working pressure. It is clearly seen that, again, continuous, smooth bead-free fibres were obtained for all cases. The surface morphology showed evenly distributed pores in the samples. K4, K5 and K6 show highly rough and undulated surface structures and the pores on the surface are less pronounced than in K1–3. The pores were also slightly elongated in the axial direction. Table 2 shows the characteristic features of the AMNP2 loaded fibres. Incidentally, AMNP2 loaded PMMA also showed a varying trend in fibre diameter with the nanoparticle concentration. 0.1% AMNP2 loaded fibres had AFD of $16 \pm 7 \mu\text{m}$, with a range of 5 μm –50 μm . 0.25% AMNP2 loaded fibres gave AFD of $12 \pm 5 \mu\text{m}$, with a range of 1 μm –40 μm . The AFD obtained for 0.5% AMNP2 loaded fibres was $7 \pm 5 \mu\text{m}$, with a range of 1 μm –35 μm .

These trends suggest that the increase of nanoparticle loadings leads to a decrease in fibre diameter. Previous studies suggested that a change in fibre diameter in pressurised gyration is owed to the combined effects of polymer concentration, rotational speed and working pressure; however, these parameters were all kept constant for each sample, thus it would be prudent to hypothesise that nanoparticle loading also affects fibre diameter. The work of Xu et al. on Ag nanoparticle incorporated

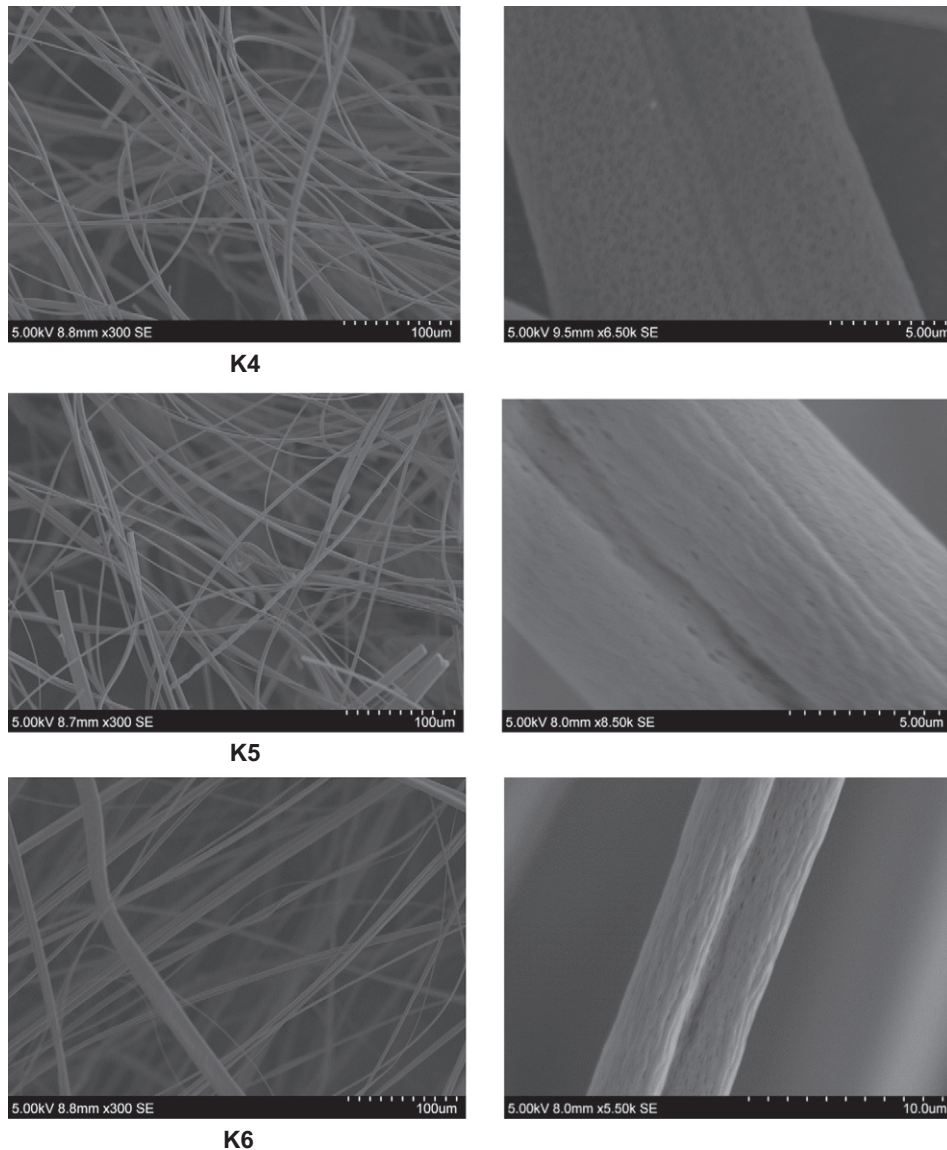


Fig. 4. SEM images of the PMMA and AMNP2 nanoparticle incorporated PMMA fibres obtained 36,000 rpm rotating speed and 0.3 MPa working pressure. K4, K5 and K6 are defined in Table 2.

nylon fibres indicated that addition of nanoparticle decreases the viscosity of the polymer solution [9]. This was due to Ag nanoparticles being dispersed in an organic solvent (triethylene glycol monomethyl ether) which acts like a surfactant in the Ag-nylon suspension. A similar argument could be applied in this scenario where addition of AMNP will act like a surfactant thus preventing strong polymer network formation. This will lower the viscosity and as a consequence the fibre diameter is lowered. However, it is also noteworthy that ambient parameters such

as temperature and humidity can also affect fibre morphology and diameters. The increase of ambient temperature favours production of the thinner fibres, e.g. as found in polyamide-6 polymer because of the inverse relationship between viscosity and temperature [26]. In addition, humidity plays a vital role in fibre diameter and morphology. Lower humidity could result in the solvent drying completely and increase the rate of solvent evaporation; on the other hand high humidity causes thicker fibre diameters to be formed [27].

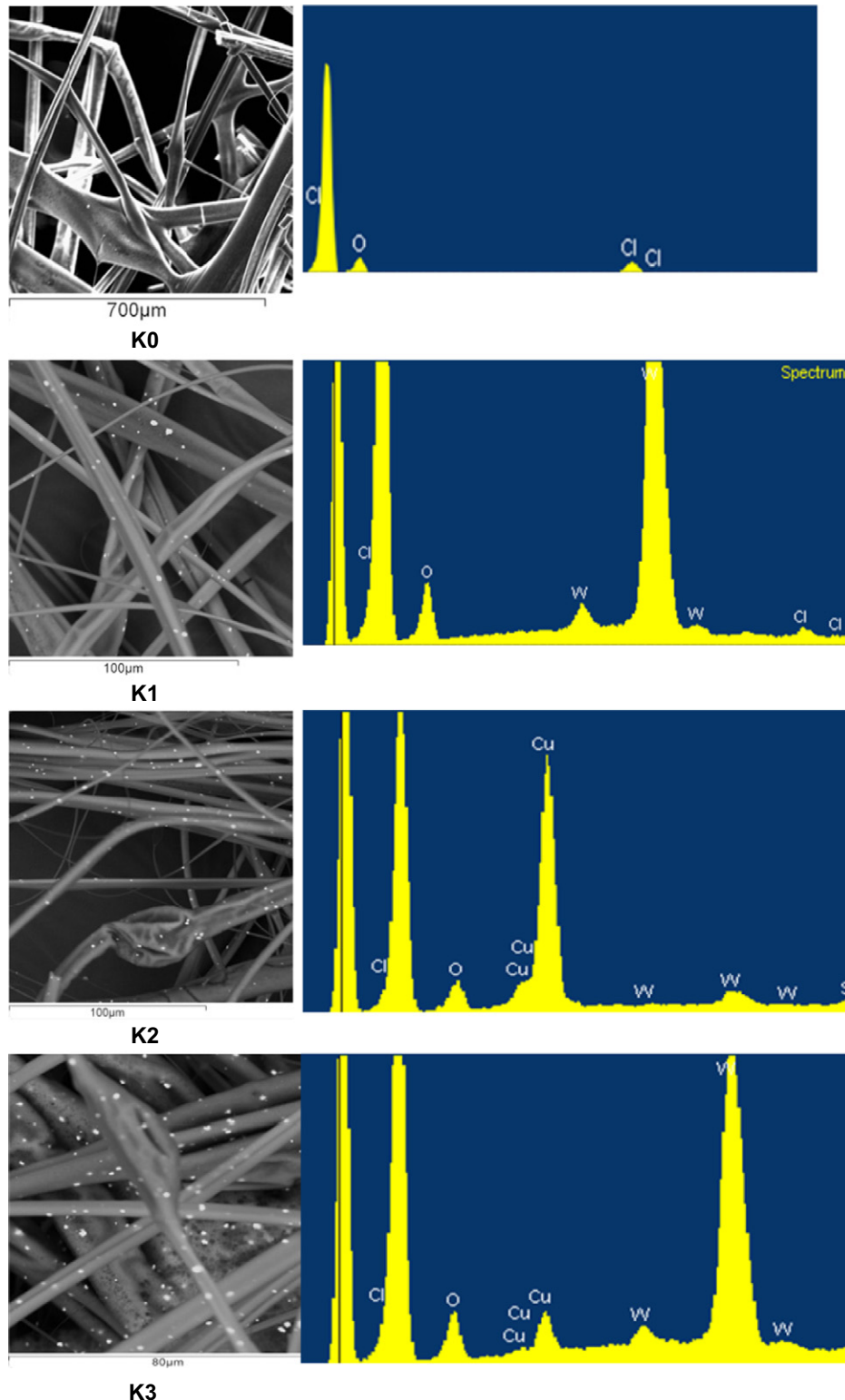


Fig. 5. EDX spectra of PMMA (K0) and composite AMNP1 loaded PMMA fibres K1–3. K1, K2 and K3 are defined in Table 1.

The APD measured for 0.1% AMNP1 loaded fibres was 67 ± 26 nm, with a range of 44 nm–200 nm. 0.25% AMNP1 fibres showed an APD of 100 ± 27 nm with a range of 32 nm–170 nm. 0.5% AMNP1 fibres exhibited an APD of 36 ± 18 nm with a range of 18 nm–149 nm. In contrast APD measured for 0.1% AMNP2 loaded fibres was 130 ± 20 nm, with a range of 60 nm–300 nm. 0.25% AMNP2 and 0.5% AMNP2 loaded fibres displayed an APD of 260 ± 35 nm and 300 ± 38 nm, respectively. The range for APD is 90 nm–430 nm and 100–480 nm for 0.25% and 0.5% AMNP2 loaded fibres, respectively.

The existence of surface pores and pore size variation with the addition of the nanoparticles could be explained in many ways. The presence of pores can be explained by the fact that chloroform was used as a solvent, a similar result can be seen in the work of Qian et al. [28] who carried out a comprehensive study on the effect of different solvents on the

morphology of electrospun PMMA fibres; fibres that had chloroform as a solvent displayed similar porous structures. Bae et al. [29] explained that with low humidity, the formed polymer jet would have less chance of coming into contact with water, whereas at higher humidity there is more chance of water vapour condensing into relatively large water droplets, allowing them to make contact with the forming jet. These water droplets can attach to the fibre surface, thus forming spherical pores on the fibre surface. With increasing humidity, the diameter and depth of the pores in the fibres will also increase. However, above a certain humidity, the quantity and depth of pores become so large that fibres do not have uniform porosity, and coalescing occurs to form large non-uniform shaped pores [27].

Pore generation in fibres could be a result of phase separation [30]. Phase separation and surface porosity in spun fibres could be due to

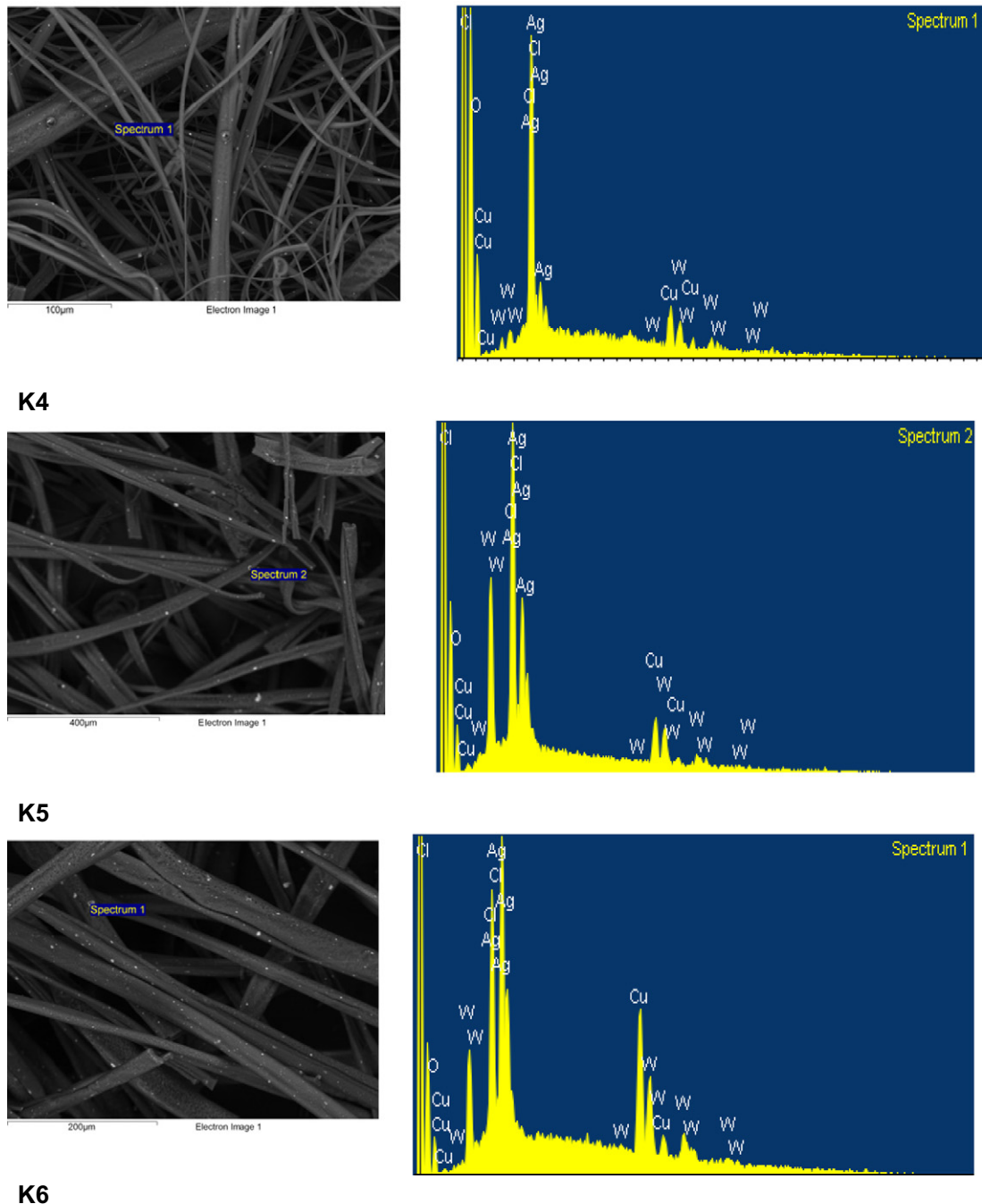


Fig. 6. EDX spectra of composite AMNP2 loaded PMMA fibres. K4, K5, K6 are defined in Table 2.

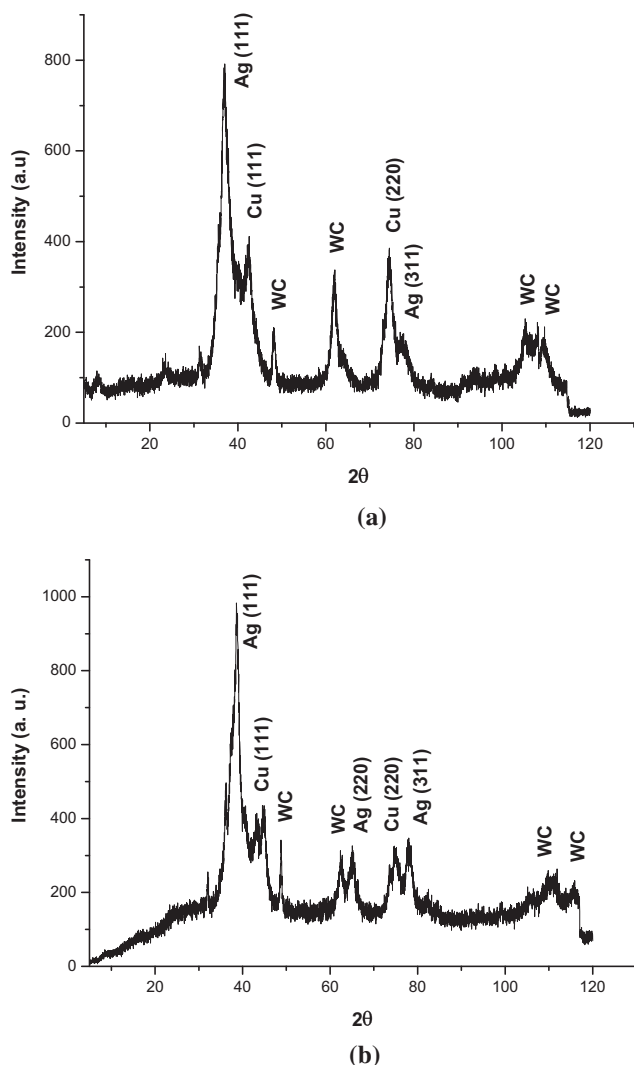


Fig. 7. XRD patterns of (a) AMNP1 (b) AMNP2 nanoparticles. Arbitrary units are indicated by a.u.

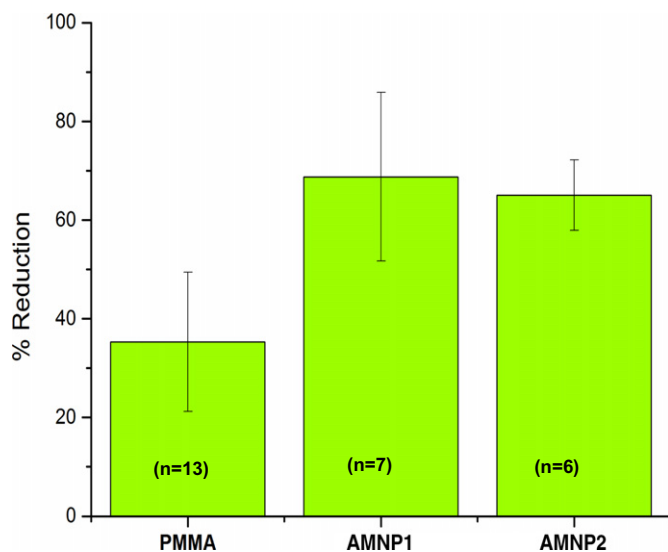


Fig. 8. Results of antimicrobial studies on AMNP loaded PMMA fibre mats K3 and K6. n indicates the number of samples tested.

high volatility solvents and related to vapour pressures [30]. By decreasing solvent volatility, porosity and smoothness of the surface of the fibres could be controlled [30]. When two solvents have different boiling points the evaporation rates of the solvents vary during the stretching and cooling process in fibre formation. This leads to a solvent-rich phase and a solvent-poor phase giving rise to the porous structure. In addition, the mixing of the polymer in a binary solvent system which consists of a good polymer solvent and a non-solvent can lead to a polymer-rich and a polymer-poor region causing phase separation to form porous structures [31]. It has been reported that the water vapour in the air could also lead to phase separation resulting in porosity in the bulk of the fibres [32]. At high humidity the water vapour which is a non-solvent to a polymer might diffuse and form liquid-liquid phase separation leading to porous structures. Moreover, the surface can develop porosity due to formation of breath figures [26]. Good miscibility of a polymer solvent and a non-solvent can facilitate precipitation during collection and solidification of nanofibres thus forming the porous structures. Blended polymeric structures have been shown to be porous by selectively removing one component from the other without controlling the ambient conditions [33]. Also, it is known that nucleation and growth during phase separation results in pores on the fibre surface, while spinodal decomposition can result in wrinkled fibre morphology [34], much like that observed in K4–6.

EDX spectroscopy was carried out in order to confirm that the nanoparticles were embedded on the surface of the composite PMMA fibres. The EDX spectra are shown in Fig. 5 for AMNP1 nanoparticle loaded PMMA fibres. The incorporation of the nanoparticles on the PMMA fibres was verified by the backscattered electrons during spectroscopy analysis. The clear contrast effect due to heavier metal particles and their compounds are seen in the micrographs and this was not observed during the secondary electron analysis of surface morphology of the virgin polymer fibres. The elements in the nanoparticles are W, Ag and Cu in case of AMNP1. In addition, S and Cl were also observed in the spectra and this might be due to the residual solvent molecules on the formed fibres. Fig. 6 exhibits the EDX spectra of AMNP2 loaded PMMA fibres obtained. Again, the main elements present in the nanoparticles are W, Ag and Cu. To verify this result X-ray diffraction studies on the AMNP nanoparticles were carried out. Fig. 7a,b show the XRD patterns of AMNP1 and AMNP2 nanoparticles. The characteristic peaks at $2\theta = 38.1^\circ$, 43.3° , 64.5° and 77.4° belong to the (111), (200), (220) and (311) crystallographic planes of fcc silver crystals [35]. Peaks observed at $2\theta = 43.3^\circ$, 50.5° and 74.1° belong to the (111), (200) and (220) crystallographic planes of copper crystals [35]. WC peaks were obtained at $2\theta = 49.1^\circ$, 62.3° , 110.2° and 115.5° [36]. This is consistent with the EDX results obtained above. The main peaks of the Ag (111), Cu (220) and WC at 62.3° were considered to calculate the composition of these elements in the nanoparticles. For that, areas of those peaks were determined by multiplying the peak height and the width at the half maximum intensity for each case. This gave an estimate of what weight percentage of each element is in the compounds [37]. Thus the weight percentage of Ag is 66%, Cu is 14% and 20% WC for the AMNP1 nanoparticles. For AMNP2 nanoparticles the weight percentages are Ag 69%, Cu 20.5% and 10.5% WC. The Ag content is almost same for both types of nanoparticles preparation. However, the Cu and WC contents vary, the Cu weight percentage is higher in AMNP2 than AMNP1 and WC shows the inverse.

3.3. Antimicrobial studies

Fig. 8 shows antimicrobial studies on PMMA and AMNP1 loaded PMMA fibres spun at 36,000 rpm rotating speed and 0.3 MPa working pressure and deposited on metal discs (Section 2.4). The antimicrobial activity of the fibres is displayed by percentage reduction of culturable *P. aeruginosa* cells with standard deviation. The pure PMMA fibres show ~35% reduction. However, the AMNP1 nanoparticle loaded fibres show ~70% reduction which is double the value of pure PMMA fibres.

Similarly, AMNP2 nanoparticle loaded fibres show ~72% reduction which is slightly higher than the previous case. The slight difference between AMNP1 and AMNP2 loaded fibres could be due to the increase in Ag and Cu contents in those samples.

Previous studies on antibacterial materials have mainly focused on metallic or nonmetallic ion-containing materials. Silver-containing coatings are a well-known example. Metallic silver has been shown to be relatively nontoxic and inert to mammalian cells while also possessing effective bactericidal abilities [8].

It is well known that the bacterial cell wall is negatively charged containing phosphatidylethanolamine (70%) as the major component. Thus, having a positively charged molecular chain in the fibres will result in an attraction of bacteria such as *P. aeruginosa* [38]. In this regard polymers with methylmethacrylate are probably the most explored kind of polymeric biocide [38]. It is generally accepted that the mechanism of the bactericidal action of the polycationic biocides involves destructive interaction with the cell wall and/or cytoplasmic membranes [39]. The above reasons are likely to have contributed to the antibacterial properties of PMMA. However, it can also be argued that the bacteria are simply trapped in the polymer mesh.

The mechanisms underlying the antibacterial activity of nanoparticles are not fully understood. Even though there are many reports proposing different mechanisms, there is no consensus. In the presence of Gram-negative bacteria, nanoparticles attach to the cell wall and disturb cell wall permeability and cell respiration [40,41]. Other studies have shown that interaction between the nanoparticle ions and the constituents of the bacterial membrane cause structural changes and damage in the cell membranes and intracellular metabolic activity, thus causing cell death [42]. The concentration of nanoparticles and the formation of “pits” in the cell wall have also been proposed as a mechanism of antibacterial activity, where the accumulation of nanoparticles in the membrane caused permeability and cell death [43,44]. All these factors are likely to have contributed to the reduction in viable cell numbers observed in AMNP loaded PMMA fibres. However, the exact mechanism for the antibacterial activity of the nanoparticles requires further investigation.

4. Conclusions

Poly(methylmethacrylate) and nanoparticle loaded poly(methylmethacrylate) fibres and fibre meshes were generated using a pressurised gyration process. The fibre diameter achieved was in the range of 6–20 µm. The pore size in the fibres was in a range 36–300 nm. The polymer concentration and the nanoparticle concentration played a key role varying the fibre size, its pore size and the morphology. Effective incorporation of the nanoparticles into the poly(methylmethacrylate) fibres was confirmed by energy dispersive X-ray analysis. X-ray analysis revealed Ag, Cu and W are the main elements in the nanoparticles. AMNP-loaded poly(methylmethacrylate) show significantly reduced numbers of Gram-negative *P. aeruginosa* cells.

Acknowledgements

This work is funded by EPSRC grants (EP/N0342281 and EP/N034368/1). The authors would like to thank Mr. John Foster (University College London, School of Pharmacy) for his assistance with making metal meshes and Dr. Tom Gregory (University College London, Department of Archaeology) for assistance with SEM and EDX microscopy.

References

- [1] E.J. Ainaissie, S.R. Penzak, M.C. Dignani, The hospital water supply as a source of nosocomial infections: a plea for action, *Arch. Intern. Med.* 162 (2002) 1483–1492.
- [2] Z. Barna, K. Antmann, J. Pászti, R. Bánfi, M. Kádár, A. Szax, M. Németh, E. Szegő, M. Vargha, Infection control by point-of-use water filtration in an intensive care unit – a Hungarian case study, *J. Water Health* 12 (2014) 858.

- [3] J. Walker, A. Jhuty, S. Parks, C. Willis, V. Copley, J. Turton, P. Hoffman, A. Bennett, Investigation of healthcare-acquired infections associated with *Pseudomonas aeruginosa* biofilms in taps in neonatal units in northern Ireland, *J. Hosp. Infect.* 86 (2014) 16–23.
- [4] J.M.C. Jefferies, T. Cooper, T. Yam, S.C. Clarke, *Pseudomonas aeruginosa* outbreaks in the neonatal intensive care unit – a systematic review of risk factors and environmental sources, *J. Med. Microbiol.* 61 (2012) 1052–1061.
- [5] C. Aumeran, C. Paillard, F. Robin, J. Kanold, O. Baud, R. Bonnet, B. Souweine, O. Traore, *Pseudomonas aeruginosa* and *Pseudomonas putida* outbreak associated with contaminated water outlets in an oncohaematology paediatric unit, *J. Hosp. Infect.* 65 (2007) 47–53.
- [6] M. Syed, S. Babar, A. Bhatti, H. Bokhari, Antibacterial effects of silver nanoparticles on the bacterial strains isolated from catheterized urinary tract infection cases, *J. Biomed. Nanotechnol.* 5 (2009) 209–214.
- [7] L. Nan, G. Ren, D. Wang, K. Yang, Antibacterial performance of Cu-bearing stainless steel against *Staphylococcus aureus* and *Pseudomonas aeruginosa* in whole milk, *J. Mater. Sci. Technol.* 32 (2016) 445–451.
- [8] U. Klueh, V. Wagner, S. Kelly, A. Johnson, J. Bryers, Efficacy of silver-coated fabric to prevent bacterial colonization and subsequent device-based biofilm formation, *J. Biomed. Mater. Res.* 53 (2000) 621–631.
- [9] Z. Xu, S. Mahalingam, J. Rohn, G. Ren, M. Edirisinghe, Physico-chemical and antibacterial characteristics of pressure spun nylon nanofibres embedded with functional silver nanoparticles, *Mater. Sci. Eng. C* 56 (2015) 195–204.
- [10] G. Borkow, Safety of using copper oxide in medical devices and consumer products, *Curr. Chem. Biol.* 6 (2012) 86–92.
- [11] H. Li, Y. Zheng, Y.T. Pei, J. de Hosson, TiNi shape memory alloy coated with tungsten: a novel approach for biomedical applications, *J. Mater. Sci. Mater. Med.* 25 (2014) 1249–1255.
- [12] M. Rai, A. Yadav, A. Gade, Silver nanoparticles as a new generation of antimicrobials, *Biotechnol. Adv.* 27 (2009) 76–83.
- [13] N. Beyth, Y. Hourí-Haddad, A. Domb, W. Khan, R. Hazan, Alternative antimicrobial approach: nano-antimicrobial materials, *Evid. Based Complement. Alternat. Med.* 1–16 (2015).
- [14] S. Mahalingam, M. Edirisinghe, Forming of polymer nanofibers by a pressurised gyration process, *Macromol. Rapid Commun.* 34 (2013) 1134–1139.
- [15] S. Mahalingam, B.T. Raimi-Abraham, D.Q.M. Craig, M. Edirisinghe, Solubility–spinnability map and model for the preparation of fibres of polyethylene (terephthalate) using gyration and pressure, *Chem. Eng. J.* 280 (2015) 344–353.
- [16] S. Mahalingam, G.G. Ren, M. Edirisinghe, Rheology and pressurised gyration of starch and starch-loaded poly(ethylene oxide), *Carbohydr. Polym.* 114 (2014) 279–287.
- [17] Z. Xu, S. Mahalingam, P. Basnett, B. Raimi-Abraham, I. Roy, D. Craig, M. Edirisinghe, Making nonwoven fibrous poly(epsilon-caprolactone) constructs for antimicrobial and tissue engineering applications by pressurized melt gyration, *Macromol. Mater. Eng.* 301 (2016) 922–934.
- [18] B.T. Raimi-Abraham, S. Mahalingam, P.J. Davies, M. Edirisinghe, D.Q.M. Craig, Development and characterization of amorphous nanofiber drug dispersions prepared using pressurized gyration, *Mol. Pharm.* 12 (2015) 3851–3861.
- [19] U.E. Illankagoon, S. Mahalingam, P. Colombo, M. Edirisinghe, Tailoring the surface of polymeric nanofibres generated by pressurised gyration, *Surf. Innov.* 4 (2016) 167–178.
- [20] A. Amir, S. Mahalingam, X. Wu, H. Porwal, P. Colombo, M.J. Reece, M. Edirisinghe, Graphene nanoplatelets loaded polyurethane and phenolic resin fibres by combination of pressure and gyration, *Compos. Sci. Technol.* 129 (2016) 173–182.
- [21] S. Mahalingam, G. Pierin, P. Colombo, M. Edirisinghe, Facile one-pot formation of ceramic fibres from preceramic polymers by pressurised gyration, *Ceram. Int.* 41 (2015) 6067–6073.
- [22] S. Zhang, B.T. Karaca, S.K. VanOosten, E. Yuca, S. Mahalingam, M. Edirisinghe, C. Tamerler, Coupling infusion and gyration for the nanoscale assembly of functional polymer nanofibers integrated with genetically engineered proteins, *Macromol. Rapid Commun.* 36 (2015) 1322–1328.
- [23] Patent PCT/GB2007/000542; World Intellectual Property Organisation 2007.
- [24] Z. Li, C. Wang, One-dimensional Nanostructures, Springer, Berlin, 2013.
- [25] X. Hong, M. Edirisinghe, S. Mahalingam, Beads, beaded-fibres and fibres: tailoring the morphology of poly(caprolactone) using pressurised gyration, *Mater. Sci. Eng. C* 69 (2016) 1373–1382.
- [26] C. Mit-uppatham, M. Nithitanakul, P. Supaphol, Ultrafine electrospun polyamide-6 fibers: effect of solution conditions on morphology and average fiber diameter, *Macromol. Chem. Phys.* 205 (2004) 2327–2338.
- [27] C.L. Casper, J.S. Stephens, N.G. Tassi, D.B. Chase, J.F. Rabolt, Controlling surface morphology of electrospun polystyrene fibers: effect of humidity and molecular weight in the electrospinning process, *Macromolecules* 37 (2004) 573–578.
- [28] Y. Qian, Y. Su, X. Li, H. Wang, C. He, Electrospinning of methyl methacrylate nanofibres in different solvents, *Iran. Polym. J.* 19 (2010) 123–129.
- [29] H. Bae, A. Haider, K.M.K. Selim, D. Kang, E. Kim, I. Kang, Fabrication of highly porous PMMA electrospun fibres and their application in the removal of phenol and iodine, *J. Polym. Res.* 20 (2013) 1–7.
- [30] S. Megelski, J.S. Stephens, D.B. Chase, J.F. Rabolt, Micro-nanostructured surface morphology on electrospun polymer fibres, *Macromolecules* 35 (2002) 8456–8466.
- [31] P. van de Witte, P.J. Dijkstra, J.W.A. van den Berg, J. Feijen, Phase separation processes in polymer solutions in relation to membrane formation, *J. Membr. Sci.* 117 (1996) 1–31.
- [32] P. Dayal, J. Liu, S. Kumar, T. Kyu, Experimental and theoretical investigations of porous structure formation in electrospun fibres, *Macromolecules* 40 (2007) 7689–7694.
- [33] M. Bognitzki, T. Frese, M. Steinhart, A. Greiner, J.H. Wendorff, A. Schaper, Preparation of fibers with nanoscaled morphologies: electrospinning of polymer blends, *Polym. Eng. Sci.* 41 (2001) 982–991.
- [34] H. Fashandi, M. Karimi, Pore formation in polystyrene fibre by superimposing temperature and relative humidity of electrospinning atmosphere, *Polymer* 53 (2012) 5832–5849.
- [35] N. Hikmah, N.F. Idrus, J. Jai, A. Hadi, Synthesis and characterisation of silver-copper core-shell nanoparticles using polyol method for antimicrobial agent, *IOP Conf. Earth Environ. Sci.* 36 (2016) 012050.
- [36] A.S. Kurllov, A.I. Gusev, Neutron and x-ray diffraction study and symmetry analysis of phase transformations in lower tungsten carbide W₂C, *Phys. Rev. B* 76 (2007) 174115.
- [37] K. Norrish, R.M. Taylor, Quantitative analysis by X-ray diffraction, *Clay Miner.* 5 (1962) 98–109.

- [38] A. Munoz-Bonilla, M. Fernandez-Garcia, Polymeric materials with antimicrobial activity, *Prog. Polym. Sci.* 37 (2012) 281–339.
- [39] E.R. Kenawy, F.I. Abdel-Hay, A.E.R.R. El-Shanshoury, M.H. El-Newehy, Biologically active polymers; synthesis and antimicrobial activity of modified poly(glycidyl methacrylate-co-2-hydroxyethyl methacrylate) derivatives with quaternary ammonium and phosphonium salts, *J. Polym. Sci. A Polym. Chem.* 40 (2002) 2384–2393.
- [40] A.M. Abdelgawad, S.M. Hudson, O.J. Rojas, Antimicrobial wound dressing nanofiber mats from multicomponent (chitosan/silver-NPs/polyvinyl alcohol) systems, *Carbohydr. Polym.* 100 (2014) 166–178.
- [41] J. An, H. Zhang, J.T. Zhang, Y.H. Zhao, X.Y. Yuan, Preparation and antibacterial activity of electrospun chitosan/(polyethylene oxide) membranes containing silver nanoparticles, *Colloid Polym. Sci.* 287 (2009) 1425–1434.
- [42] W.K. Jung, H.C. Koo, K.W. Kim, S. Shin, S.H. Kim, Y.H. Park, Antibacterial activity and mechanism of action of the silver ion in *Staphylococcus aureus* and *Escherichia coli*, *Appl. Environ. Microbiol.* 74 (2008) 2171–2178.
- [43] I. Sondi, B. Salopek-Sondi, Silver nanoparticle as antibacterial agent: a case study on *E. coli* as a model for Gram-negative bacteria, *J. Colloid Interface Sci.* 275 (2004) 177–182.
- [44] Y.Z. Zhou, J. Yang, T.T. He, H.F. Shi, X.N. Cheng, Y.X. Lu, Highly stable and dispersive silver nanoparticle-graphene composites by a simple and low-energy-consuming approach and their antimicrobial activity, *Small* 9 (2013) 3445–3454.



U. Eranka Illangakoon gained his PhD from School of Pharmacy - University College London (UCL) in 2016. His thesis was entitled “Advanced drug delivery systems prepared by electrospinning”. He also holds a MBA from University of East London and MSc Pharmaceutical Science from London Metropolitan University. After his PhD he joined UCL Mechanical Engineering as a postdoctoral researcher. Currently he focus on making various biomaterials and smart drug delivery systems using pressurised gyration and electrospinning.



S. Mahalingam gained his doctorate from UCL. Subsequently, he was a research associate in the Interface Analysis Centre at Bristol University, UK. Currently, he is an Engineering & Physical Sciences Research Council (UK) supported research associate in the Department of Mechanical Engineering at UCL where he is inventing techniques to manufacture functional polymeric fibres and smart bubbles across the scale range from micro-nano mainly for pharmaceutical and biomedical applications. He won the 2014 Materials Science & Engineering C Young Researcher Award.



K. Wang recently gained a Master of Science degree in Biomaterials and Tissue Engineering from UCL, for which she gained a distinction. She also graduated with a Bachelor of Science degree in Biomedical Sciences from Brunel University, London, UK. Her interests lie in integrating engineering and biomedicine for medical applications and she is currently looking to pursue a PhD to further her career in industry.



Y.-K. Cheong is an EPSRC research fellow in the School of Engineering and Technology at University of Hertfordshire. She is a UK Royal Society of Chemistry Chartered Chemist. She graduated with MSc in Pharmaceutical Chemistry. After the completion of her PhD in Chemistry at Queen Mary University of London, she worked on several Global Engineering loyalty funded projects related to applied phosphorus chemistry and syntheses of imaging reagents for nuclear medicine. Y.-K. is currently focusing her research in nanomaterials characterisations, their surface treatments and modification through organometallic conjugations using novel ligands.



E. Canales joined UCL in 2009. Her career has largely been in the arena of clinical microbiology and quality control in biotechnology/radiopharmaceutical industries. She completed her PhD from University of Zaragoza, Spain on the “The molecular epidemiology of the resistance to macrolide antibiotics in *Streptococcus pneumoniae*”. Her research interests lie in understanding how different engineering technologies can help to reduce the spread of infectious diseases in indoor environments, the study of individual microorganisms and microbial communities’ interaction with various environments, discovery and development of new antimicrobial agents.



G.G. Ren is a Senior Lecturer at School of Engineering and Technology, University of Hertfordshire, UK. He holds a BSc/BEng in Organic Chemical Engineering (China) and a PhD in Materials from Queen Mary University of London. He has been investigating functional nanomaterials, particularly antimicrobial nanoparticles (AMNP) since 2000. He is now exploring the healthcare applications of the AMNP with an aim to prevent transmission of infectious diseases in hospitals. His current interests also cover dispersing nanoparticles into biological and engineering fluids, and synthesis of chemical nanoconjugates for bone and cancer disease control in biomedical applications.



E. Cloutman-Green has worked as a Healthcare Scientist in Infection Prevention and Control (IP&C) at Great Ormond Street Hospital since 2007. In 2010 she was awarded an NIHR CSO Doctoral Fellowship during which she completed a PhD on ‘The role of the environment in transmission of healthcare associated infection’. In 2015 she successfully attained Fellowship of the Royal College of Pathologists and in 2016 her research in IP&C led to her being awarded an NIHR ICA Clinical Lectureship. She is currently both the Chair of the Environmental Network and a NICE Expert Advisor in IP&C.



M. Edirisinghe FEng, holds the Bonfield Chair of Biomaterials in the Department of Mechanical Engineering at University College London. He has published over 350 journal papers and his most recent research is on creating novel techniques for the preparation of particles, bubbles, capsules and fibres. Together with Dr. Mahalingam, they invented pressurised gyration and other related sister-processes to manufacture novel polymeric structures. He has been awarded many prizes for his research including the Royal Society Brian Mercer Feasibility Award for an unprecedented three times (2005, 2009 and 2013).



L. Ciric’s research focuses on the profiling of microbial communities in various environments, and bacterial antibiotic resistance mechanisms and their modes of transfer among different communities. Lena is interested in the discovery of novel antimicrobial strategies. She manages the Healthy Infrastructure Research Group (, www.cege.ucl.ac.uk/HIRG) at UCL Civil Environmental and Geomatic Engineering, investigating engineering solutions that reduce the spread of infectious disease and improve environmental health.